Change in the magnetic structure of (Bi,Sm)FeO3 thin films at the morphotropic phase boundary probed by neutron diffraction

Shingo Maruyama, Varatharajan Anbusathaiah, Amy Fennell, Mechthild Enderle, Ichiro Takeuchi, and William D. Ratcliff

Citation: APL Materials **2**, 116106 (2014); doi: 10.1063/1.4901294
View online: http://dx.doi.org/10.1063/1.4901294
View Table of Contents: http://scitation.aip.org/content/aip/journal/aplmater/2/11?ver=pdfcov
Published by the AIP Publishing

APL MATERIALS **2**, 116106 (2014)

Change in the magnetic structure of (Bi,Sm)FeO_3 thin films at the morphotropic phase boundary probed by neutron diffraction

Shingo Maruyama,[1] Varatharajan Anbusathaiah,[1] Amy Fennell,[2] Mechthild Enderle,[3] Ichiro Takeuchi,[1] and William D. Ratcliff[4,a]
[1]*Department of Materials Science and Engineering, University of Maryland, College Park, Maryland 20742, USA*
[2]*Paul Scherrer Institut, 5232 Villigen PSI, Switzerland*
[3]*Institut Laue Langevin, BP 156, 38042 Grenoble, France*
[4]*NIST Center for Neutron Research, National Institute of Standards and Technology, Gaithersburg, Maryland 20899, USA*

(Received 25 July 2014; accepted 27 October 2014; published online 12 November 2014)

We report on the evolution of the magnetic structure of $BiFeO_3$ thin films grown on $SrTiO_3$ substrates as a function of Sm doping. We determined the magnetic structure using neutron diffraction. We found that as Sm increases, the magnetic structure evolves from a cycloid to a G-type antiferromagnet at the morphotropic phase boundary, where there is a large piezoelectric response due to an electric-field induced structural transition. The occurrence of the magnetic structural transition at the morphotropic phase boundary offers another route towards room temperature multiferroic devices. [http://dx.doi.org/10.1063/1.4901294]

As one of the only single-phase multiferroic materials with ferroelectric and magnetic transition temperatures well above room temperature, $BiFeO_3$ (BFO) has been extensively studied. It possesses a robust ferroelectric polarization which is closely tied to its rhombohedral structure, and microstructural properties of BFO thin films (such as the stress state, grain size and its orientation) can sensitively affect its local ferroelectric properties. Magnetoelectric coupling between the local ferroelectric polarization and magnetism inside BFO thin films can serve as the basis for heterostructured multiferroic devices,[1,2] but their antiferromagnetic properties are known to display complex variations depending delicately on the local microstructural properties. We have previously used neutron diffraction to probe the nature of antiferromagnetic domains in epitaxial BFO thin films.[3,4]

Chemical substitution in BFO has been explored in order to improve the ferroelectric, piezoelectric, dielectric, and magnetic properties of the material.[5–16] It has been demonstrated that the substitution of rare earth elements into the A-site of BFO thin films results in a structural phase transition from a ferroelectric rhombohedral phase to a paraelectric orthorhombic phase.[7–9,14,15] In the case of Sm, the transition occurs at ~14% doping[17–20] at which point films exhibit a Morphotropic Phase Boundary (MPB). Earlier studies showed that in the vicinity of the MPB, an electric field can be used to drive the transition from the paraelectric orthorhombic phase to the rhombohedral ferroelectric phase, resulting in a very large piezoelectric effect d_{33} larger than 150 pm/V.[21] Since the ferroelectric and magnetic domains are coupled in this compound,[4,22–24] the change of the magnetic structure across the phase boundary can potentially serve as another avenue for a multiferroic device operation. While there are some reports on the magnetic structure of bulk doped BFO,[13–16] the information of the magnetic structures in doped BFO thin films is scarce. In this study, we determined the magnetic structure of Sm-doped BFO films grown on a $SrTiO_3$ (STO) substrate using

[a]Author to whom correspondence should be addressed. Electronic mail: william.ratcliff@nist.gov

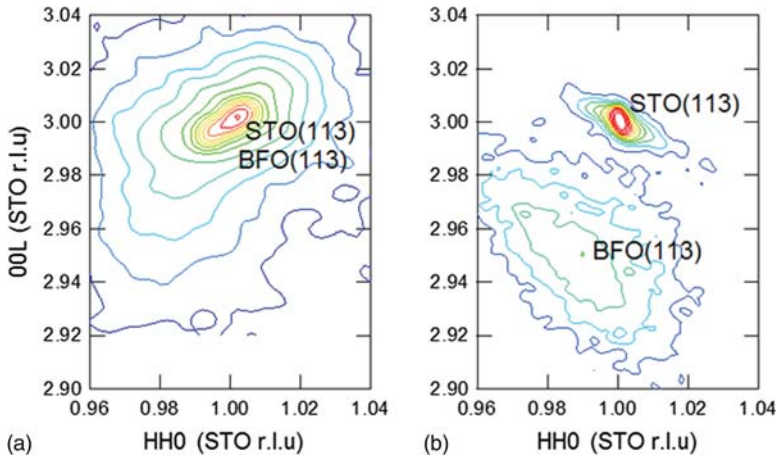

FIG. 1. X-ray reciprocal space mappings around STO (113) Bragg reflections taken for (a) 840 nm thick 10.4% Sm-doped BFO and (b) 1 μm thick 18.7% Sm-doped BFO films grown on miscut STO (001) substrate. Note that the peaks in 10.4% Sm-doped BFO are overlapping due to the small lattice mismatch.

polarized neutron diffraction. We show that the magnetic structure is sensitive to Sm doping. For Sm concentration less than ~14%, indications for a cycloid were found, while for Sm concentration more than ~14%, a G-type collinear magnetic order was observed.

BFO films grown on a (0 0 1) STO substrate show four equivalent crystallographic domains based on the four different quasi-cubic body diagonals, which complicate the determination of the magnetic structure. In order to simplify our investigation of the magnetic structure Sm-doped BFO films, we used (0 0 1) STO substrates with a 4° miscut along [1 1 0] direction on which we can obtain single ferroelectric domain BFO films.[25,26] The Sm-doped BFO films are grown epitaxially by Pulsed Laser Deposition (PLD) with alternating deposition of Bi-rich BFO and $SmFeO_3$ targets onto the ~50 nm $SrRuO_3$ (SRO) buffered miscut (0 0 1) STO substrates. Deposition thickness in one cycle is about a half unit cell of BFO pseudo cubic lattice for each target to ensure the uniform mixing of the dopant in the BFO film. The thicknesses of the Sm doped BFO films are ~840 nm for the 10.4% Sm-doped BFO film and ~1 μm for the 16.1% and 18.7% Sm-doped BFO films. The epitaxial relationship between the film and the substrate was determined through the use of X-ray reciprocal space maps (RSMs). We characterized the ferroelectric domain structures of the films using conventional Piezoresponse Force Microscopy (PFM) in an area of 5 μm^2. All films show no piezoresponse contrast in either the out-of-plane or the in-plane directions. Since ferroelectric thin films are obtained at the Sm concentration below the MPB, no piezoresponse contrast at 10.4% Sm doping indicates that the film has a ferroelectric monodomain structure in the observed area (5 μm^2). This is consistent with energetic considerations.[27] Since the paraelectric phases at 16.1% and 18.7% Sm doping do not have any piezoelectric effect, there is no contrast.[17]

Neutron diffraction measurements were performed on the BT-4 and BT-7 triple-axis spectrometers (NIST Center for Neutron Research); the IN20 thermal triple-axis spectrometer (ILL, France); and the cold triple-axis spectrometer TASP (PSI, Switzerland). The measurements on BT-7,[28] IN20, and TASP employed polarized neutrons, and IN20 and TASP were equipped with the "zero magnetic field" environments CryoPAD[29] and MuPAD,[30] respectively. The zero-field environments allow the arbitrary orientation of the neutron polarization and as such all scattering cross-sections can be measured. Polarized neutron measurements allow a direct measurement of the orientation of a magnetic moment in the scattering plane and can be used to identify a magnetic structure that is composed of two out of phase components, i.e., a cycloidal structure gives a different response to an amplitude modulated structure with the same periodicity. All measurements were done at room temperature.

Fig. 1 shows the X-ray RSMs taken for 10.4% and 18.7% Sm-doped BFO films. We see there is one broad reflection for Sm concentrations less than or more than the MPB concentration (~14% Sm). For the 10.4% doping sample, the peak separation due to the crystallographic domains would

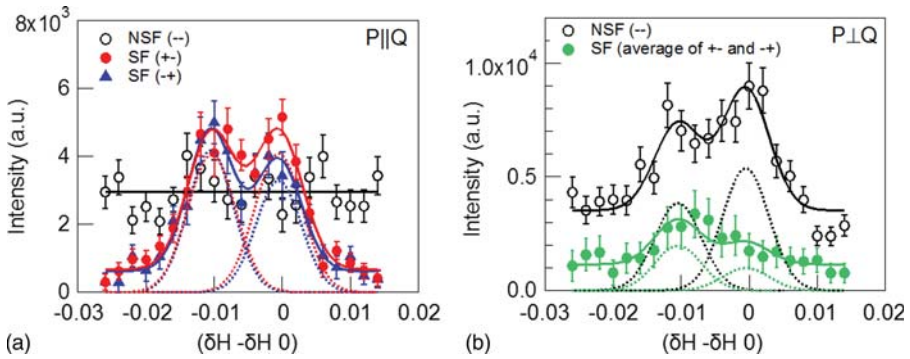

FIG. 2. Polarized neutron diffraction measurements of the 10.4% Sm-doped BFO film. Intensity profiles are taken in (H K (H + K)/2) zone with (a) P (neutron polarization)||Q (scattering vector) and (b) P⊥Q. Open circles indicate NSF and close circles and triangles indicate SF scattering. Horizontal axes indicate the displacement from (0.5 0.5 0.5) reflection. Since we index within the reference frame of the substrate, the offset in H from $\delta = 0$ is due to an imperfect lattice match/epitaxy. Error bars are statistical in nature and represent one standard deviation. Solid lines represent fits to the data to two Gaussians and a background and dotted lines represent the Gaussian contribution to the fits.

be smaller than the broadness of the BFO peak of this sample because the distortion angle along [1 1 0] direction in the sample with 10.4% Sm doping is ~89.8°.[10] Based on the fact that the PFM shows no contrast for this sample and BFO prefers to grow in a single domain on miscut STO along [1 1 0] shown in the previous studies,[25,26] we treat this film as having a quasi-single crystallographic domain. For the 18.7% Sm-doped BFO film, since the difference of a_{orth} and b_{orth} would be ~3% for this orthorhombic phase,[11] the peak separation should be seen if the film has multiple crystallographic domains. That only one peak is observed in Fig. 1(b) indicates that the film only has a single crystallographic domain.

For the 10.4% Sm-doped BFO film, which has a Sm concentration less than the MPB, in the ferroelectric rhombohedral phase, we focused on the magnetic reflections observed near the (0.5 0.5 0.5) reciprocal lattice position (we use pseudocubic indexing throughout this paper). The reflection lies in the (H K (H + K)/2) scattering plane, which is defined by the (1 1 1) and (1 −1 0) reflections. Fig. 2(a) shows polarized diffraction measurements of Spin-Flip (SF) and Non-Spin-Flip (NSF) scatterings with the neutron polarization parallel or anti-parallel to the scattering vector, Q. In this figure, we see that SF scattering (+− and −+) shows two peaks, while the NSF scattering shows no peak. Therefore, these peaks have an entirely magnetic origin. The slightly incommensurate peak positions (with respect to the film) indicate the presence of either an amplitude modulated or cycloidal magnetic structure. Reciprocal space maps made in this scattering plane (see supplementary material[31]) indicate that the propagation direction is along (1 −1 0). Here, the separation between peaks is 0.099(3) rlu for the SF(−+) scattering which is consistent with a delta ~0.0049(2). This is in agreement with the reported value in bulk of 0.0045 rlu, given that we are indexing within the coordinate system of the substrate. This separation is consistent with the presence of a single magnetic domain[4] (if multiple magnetic domains were present, given the wide vertical resolution of a triple axis, the separation between the peaks would be much less.) The clear difference between +− and −+ scattering, observed for one of the peaks, excludes a modulated collinear structure. Fig. 2(b) shows SF and NSF scatterings with the neutron polarization out of the scattering plane. In this figure, we see that the NSF scattering has two peaks, with weaker scattering in the SF channels. In fact, the in-plane component is about $1/\sqrt{5}$ of the component out of the plane, since the SF:NSF intensities are ~1:5. This shows that the cycloid (elliptic or circular), when projected perpendicular to Q, has a significantly larger component along the out-of-plane direction (1 1 −2) than in the plane, along (1 −1 0). This points to either a tilted plane for the cycloid or to an elliptical skewing of the cycloid. We note that the results in Fig. 2(b) are completely unaffected by the presence or absence of "magnetic polarity domains" (cycloids are manifestly not chiral). However, if we define a coordinate system based on the propagation vector and the ferroelectric polarization, then there can be a rotation sense associated with the cycloid in this coordinate system. A magnetic polarity domain is a domain with one of these rotation

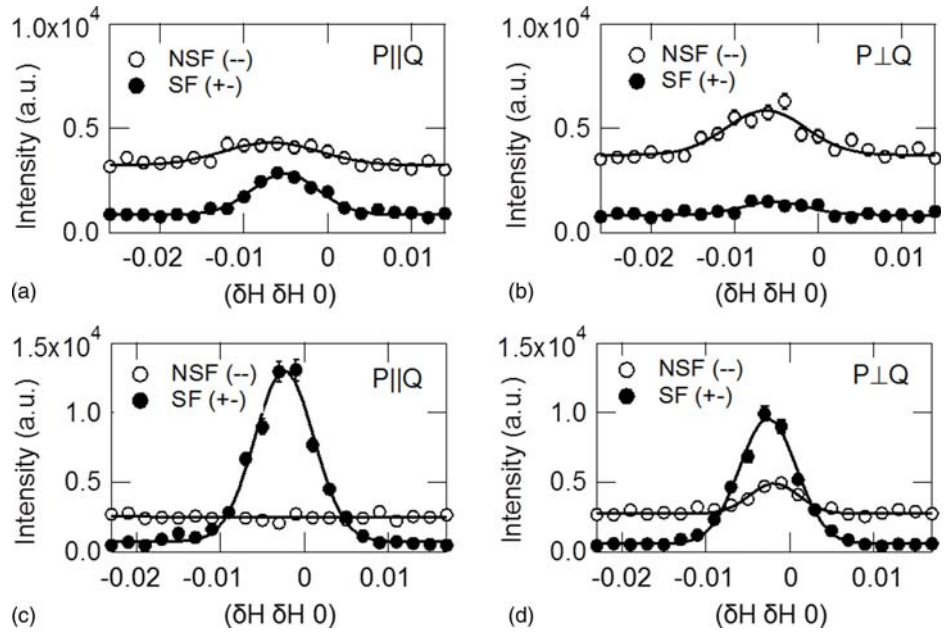

FIG. 3. Polarized neutron diffraction measurements of the 16.1% Sm-doped BFO film. Intensity profiles are taken in the (HHL) zone with (a) P||Q and (b) P⊥Q about the (0.5 0.5 0.5), and (c) P||Q and (d) P⊥Q about the (0.5 0.5 −0.5) position. Horizontal axes in (a) and (b), and (c) and (d) indicate the displacement from (0.5 0.5 0.5) and (0.5 0.5 −0.5) reflections, respectively. Since we index within the reference frame of the substrate, the offset in H from $\delta = 0$ is due to an imperfect lattice match/epitaxy. Open circles indicate NSF, and close circles and triangles indicate SF scattering. Error bars are statistical in nature and represent one standard deviation. Solid lines represent Gaussian fits to the data.

senses. In neutron scattering, the horizontal (P||Q) spin flip cross section has a $\pm\langle(\hat{P}\cdot(\overrightarrow{M_\perp}\wedge\overrightarrow{M_\perp^*}))\rangle$ term,[32] where the sign is determined based on whether we are considering the +− or −+ channel, $\overrightarrow{M_\perp}(\vec{Q}) \propto \sum_j f_j(\vec{Q})\overrightarrow{m_{\perp j}}e^{i\vec{Q}\cdot\vec{r_j}}$, $\overrightarrow{m_{\perp j}}$ denotes the spin on a given site that is perpendicular to the position in reciprocal space, $\vec{Q}$, $f_j(\vec{Q})$ is the Fourier transform of the magnetization density at the site j, and $\overrightarrow{P}$ denotes the neutron polarization. If there is a single magnetic polarity domain, this will manifest itself in the scattering as a complete asymmetry in the +− and −+ channels of the cross section if we measure in a plane where the neutron polarization is parallel to the rotation axis of the cycloid. In this scenario, in one cross section, we would expect to see a single "satellite" in each channel, one to the left and one to the right of the (0.5 0.5 0.5) position.

Now, if there was a single polarity domain, the −+:+− intensity ratio in Fig. 2(a) should roughly go as 1:7. However, it is more like 4:5 (at least for the left hand peak). These two observations point to near-equally populated magnetic polarity domains regardless of whether the cycloid is tilted or elliptically skewed.

Spherical Neutron Polarimetry (SNP) measurements undertaken on TASP with MuPAD could not fully resolve the details of the magnetic structure. However, the scattering shown in Fig. 2 (measured on BT-7) and measured on TASP indicates that the magnetic structure has components parallel to (1 1 −2) as well as along (1 −1 0). Thus, while we cannot say with certainty whether the magnetic structure is better described by a circular cycloid which is tilted, or by one which is, elliptically skewed, the data do indicate a cycloidal magnetic structure, with a spin-plane different from the one found in the undoped BFO crystal but consistent with that found in undoped BFO thin films.[4]

Next, we turn to the film with Sm concentration greater than the MPB, which is in the paraelectric orthorhombic phase. Fig. 3 shows our polarized neutron diffraction measurements for the 16.1% Sm-doped BFO film. This time, we oriented the film in the (H H L) scattering plane, which is defined by the (1 1 0) and (0 0 1) reflections. We show SF and NSF measurements on the magnetic reflection around the (0.5 0.5 0.5) position with the neutron polarization P parallel to the scattering

TABLE I. Integrated intensity of the peaks on the magnetic reflections (0.5 0.5 0.5) and (0.5 0.5 −0.5) of the 16.1% Sm-doped BFO film shown in Fig. 3.

	P||Q		P⊥Q	
Magnetic reflection	NSF(−−)	SF(+−)	NSF(−−)	SF(+−)
(0.5 0.5 0.5)	15.6 ± 2.7	19.3 ± 1.2	25.5 ± 3.5	6.1 ± 1.2
(0.5 0.5 −0.5)	0	108.4 ± 4.1	15.8 ± 1.1	76.3 ± 2.3

vector Q (Fig. 3(a)). A single peak is observed for the SF and NSF configurations, indicating that there is a (0.5 0.5 0.5) ordering wave vector present, which implies G-type antiferromagnetic order. When P is out of the scattering plane as shown in Fig. 3(b), the SF and NSF scatterings also show a single peak. This result indicates that the moments have components along [1 −1 0] and [1 1 −2]. Since we are not able to restrict the moment in the HHL plane only from (0.5 0.5 0.5) reflection due to the insensitivity of magnetic neutron scattering to components of the moment along the scattering vector, [1 1 1], we also measured (0.5 0.5 −0.5) reflection to determine the moment as shown in Figs. 3(c) and 3(d). SF scattering at P||Q (Fig. 3(c)), NSF and SF scatterings at P⊥Q (Fig. 3(d)) show a single peak, indicating the moment has components along [−1 1 0] and [1 1 2]. We determine the integrated intensities of the magnetic scattering peaks from (0.5 0.5 0.5) and (0.5 0.5 −0.5) by fitting as shown in Fig. 3 after correcting for depolarization of the ^{3}He cell (Table I). Then, the possible orientation of the magnetic moment has been extracted by fitting those integrated intensities (of all measured cross-sections) using a Bayesian fitting routine, the moment has the angle $\varphi = 15.1(2)^\circ$ from [1 0 0] and $\theta = 56.1(4)^\circ$ from [0 0 1] direction.

We also measured the higher Sm-doped BFO film with 18.7% Sm doping using Cryopad at ILL. The fit to the polarization matrix data measured at the magnetic reflections (0.5 0.5 0.5) and (0.5 0.5 −0.5) was undertaken with MuFit,[33] and is shown in Table II. The magnetic structure of the film is also a G-type collinear structure. The best fit gave an orientation of the magnetic moment of $\varphi = 31.4(4)^\circ$ from [1 0 0] and $\theta = 43.8(2)^\circ$ from [0 0 1]. While we initially attempted to fit our data to a model consisting of single domains, such fits were poor (even using simulated annealing) and we switched to a model allowing magnetic domains of unequal population. As the film is orthorhombic in this phase, we allowed 4 domains. There is the original domain (abc → abc), one in which the direction along the crystallographic a-axis is inverted (a → −a), (b → −b), and (c → −c). We found the sample consisted of the following domains: 6(1)% (abc → abc), 3(1)% (c → −c), 13(3)% (b → −b), and 78(16)% (a → −a) with chi squared of ~0.53. We assume that this particular distribution of domains is accidental, though the strong preference for "a → −a" type domains is intriguing.

In Fig. 4, we summarize the evolution of the possible magnetic structures with Sm doping in the relatively thick (~1 μm) BFO films grown on miscut (0 0 1) STO substrates across the MPB. For the non-doped BFO film, the recovery of the cycloidal structure with a different chirality axis from bulk was found as we reported previously.[4] The 10.4% Sm-doped BFO, which has a Sm concentration less than the MPB, has a chiral magnetic structure propagating along (1 −1 0) with

TABLE II. Polarization matrix data observed on the magnetic reflections (0.5 0.5 0.5) and (0.5 0.5 −0.5) of the 18.7% Sm-doped BFO film using Cryopad.

		Pout (measurement)			Pout (calculated)		
Magnetic reflection	Pin	x	y	z	x	y	z
(0.5 0.5 −0.5)	x	−0.95(10)	0.01(5)	0.01(5)	−1	0	0
	y	−0.02(5)	−0.07(7)	−0.52(8)	0	−0.14	−0.52
	z	0.01(5)	−0.52(8)	0.21(7)	0	−0.52	0.14
(0.5 0.5 0.5)	x	−1.04(16)	−0.05(7)	−0.10(8)	−1	0	0
	y	−0.08(8)	−0.1(1)	−0.76(14)	0	0.01	−0.75
	z	0.00(100)	−0.75(14)	−0.08(11)	0	−0.75	0.01

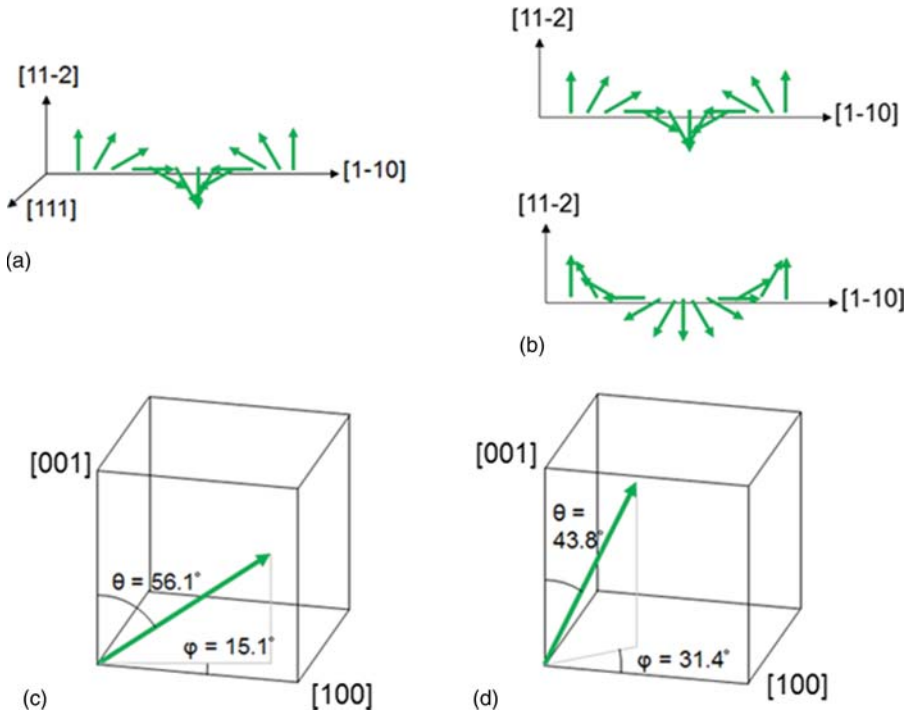

FIG. 4. Cartoon of possible magnetic structures for Sm-doped BFO films with Sm content of (a) 0% with a spin cycloid, (b) 10.4%, a cycloid with two chirality domains, (c) 16.1%, a G-type antiferromagnet, and (d) 18.7%, a G-type antiferromagnet.

a component along both [1 −1 0] and [1 1 −2] directions. With concentrations greater than the MPB, at 16.1% and 18.7% Sm doping, the magnetic structure changes to a collinear G-type antiferromagnetic order, however the moment lies along different directions at different doping. These results indicate that the magnetic structure in the Sm-doped BFO film is very sensitive to the doping concentration. The change of the magnetic structure is consistent with the previous reports on bulk rare earth doped BFO,[13,16] indicating that the magnetic structure is likely tightly linked to changes in the lattice. In the rhombohedral phase, the magnetic order is basically G-type, with a long-range cycloidal modulation induced through the Dzyaloshinskii-Moriya interaction, which is allowed by the symmetry of the polar phase. However, in the paraelectric centrosymmetric orthorhombic phase, this interaction is no longer allowed and, thus, we can expect G-type ordering. A recent study on epitaxial BFO thin films with thickness of 70 nm on different substrates suggests that the magnetic structure changes drastically with small epitaxial strains.[34] Theoretical predictions,[35] also show that the cycloid is extremely sensitive to strain. Furthermore, with Sm doping, both the Fe–O–Fe bond angle, as well as the lattice parameters shift, which could serve to change the single ion anisotropy direction and, thus, the direction of the ordered moment that we observed in the G-type antiferromagnetic samples.[36] All of these are consistent with our finding that the crystal and magnetic structures in these materials are tightly coupled. Both strain and chemical pressure can change the crystal structure and thus the magnetic structure of these materials.

In summary, we find that the doping of Sm into BFO thin films has a dramatic effect on its magnetic structure. As the Sm concentration increases, the magnetic structure evolves from a cycloid to a G-type antiferromagnet. Even within the G-type phase, the direction of the ordered moment changes. At the MPB, an electric-field-induced transformation from a paraelectric orthorhombic phase to the ferroelectric rhombohedral phase was suggested in our previous report.[8] Thus, Sm doping would allow one to tune the magnetic structure of the paraelectric phase. This phase could then be driven with an electric field back to the rhombohedral ferroelectric phase with cycloidal

magnetic order. This opens the door to greater control magnetolectric devices across the phase boundary.

We acknowledge the support of the National Institute of Standards and Technology and U.S. Department of Commerce through Grant No. 70NANB7H6177 and in providing neutron research facilities used in this work. The work was also supported by the W. M. Keck Foundation. Bayesian fitting of the polarized neutron diffraction data at NIST was done using BUMPS developed by Paul Kienzle (NIST).

[1] R. Ramesh and N. A. Spaldin, Nat. Mater. **6**, 21 (2007).
[2] J. Allibe, S. Fusil, K. Bouzehouane, C. Daumont, D. Sando, E. Jacquet, C. Deranlot, M. Bibes, and A. Barthélémy, Nano Lett. **12**, 1141 (2012).
[3] W. Ratcliff, D. Kan, W. Chen, S. Watson, S. Chi, R. Erwin, G. J. McIntyre, S. C. Capelli, and I. Takeuchi, Adv. Funct. Mater. **21**, 1567 (2011).
[4] W. Ratcliff, Z. Yamani, V. Anbusathaiah, T. Gao, P. Kienzle, H. Cao, and I. Takeuchi, Phys. Rev. B: Condens. Matter Mater. Phys. **87**, 140405 (2013).
[5] H. Ishiwara, Curr. Appl. Phys. **12**, 603 (2012).
[6] C.-H. Yang, D. Kan, I. Takeuchi, V. Nagarajan, and J. Seidel, Phys. Chem. Chem. Phys. **14**, 15953 (2012).
[7] S. Fujino, M. Murakami, V. Anbusathaiah, S.-H. Lim, V. Nagarajan, C. J. Fennie, M. Wuttig, L. Salamanca-Riba, and I. Takeuchi, Appl. Phys. Lett. **92**, 202904 (2008).
[8] D. Kan, L. Pálová, V. Anbusathaiah, C. J. Cheng, S. Fujino, V. Nagarajan, K. M. Rabe, and I. Takeuchi, Adv. Funct. Mater. **20**, 1108 (2010).
[9] C.-J. Cheng, D. Kan, V. Anbusathaiah, I. Takeuchi, and V. Nagarajan, Appl. Phys. Lett. **97**, 212905 (2010).
[10] D. Kan, V. Anbusathaiah, and I. Takeuchi, Adv. Mater. **23**, 1765 (2011).
[11] D. Kan, C.-J. Cheng, V. Nagarajan, and I. Takeuchi, J. Appl. Phys. **110**, 014106 (2011).
[12] D. Kan, C. J. Long, C. Steinmetz, S. E. Lofland, and I. Takeuchi, J. Mater. Res. **27**, 2691 (2012).
[13] I. Sosnowska, M. Loewenhaupt, W. I. F. David, and R. M. Ibberson, Mater. Sci. Forum **133-136**, 683 (1993).
[14] Z. V. Gabbasova, M. D. Kuz'min, A. K. Zvezdin, I. S. Dubenko, V. A. Murashov, D. N. Rakov, and I. B. Krynetsky, Phys. Lett. A **158**, 491 (1991).
[15] I. Levin, S. Karimi, V. Provenzano, C. L. Dennis, H. Wu, T. P. Comyn, T. J. Stevenson, R. I. Smith, and I. M. Reaney, Phys. Rev. B: Condens. Matter Mater. Phys. **81**, 020103 (2010).
[16] I. Levin, M. G. Tucker, H. Wu, V. Provenzano, C. L. Dennis, S. Karimi, T. Comyn, T. Stevenson, R. I. Smith, and I. M. Reaney, Chem. Mater. **23**, 2166 (2011).
[17] A. Y. Borisevich, E. A. Eliseev, A. N. Morozovska, C.-J. Cheng, J.-Y. Lin, Y. H. Chu, D. Kan, I. Takeuchi, V. Nagarajan, and S. V. Kalinin, Nat. Commun. **3**, 775 (2012).
[18] S. B. Emery, C.-J. Cheng, D. Kan, F. J. Rueckert, S. P. Alpay, V. Nagarajan, I. Takeuchi, and B. O. Wells, Appl. Phys. Lett. **97**, 152902 (2010).
[19] C.-J. Cheng, D. Kan, S.-H. Lim, W. McKenzie, P. Munroe, L. Salamanca-Riba, R. Withers, I. Takeuchi, and V. Nagarajan, Phys. Rev. B: Condens. Matter Mater. Phys. **80**, 014109 (2009).
[20] C.-J. Cheng, A. Y. Borisevich, D. Kan, I. Takeuchi, and V. Nagarajan, Chem. Mater. **22**, 2588 (2010).
[21] S. Yasui, P. Maksymovych, and I. Takeuchi, private communication (2014).
[22] T. Zhao, A. Scholl, F. Zavaliche, K. Lee, M. Barry, A. Doran, M. P. Cruz, Y. H. Chu, C. Ederer, N. A. Spaldin, R. R. Das, D. M. Kim, S. H. Baek, C. B. Eom, and R. Ramesh, Nat. Mater. **5**, 823 (2006).
[23] S. Lee, W. Ratcliff, S.-W. Cheong, and V. Kiryukhin, Appl. Phys. Lett. **92**, 192906 (2008).
[24] S. Lee, T. Choi, W. Ratcliff, R. Erwin, S.-W. Cheong, and V. Kiryukhin, Phys. Rev. B: Condens. Matter Mater. Phys. **78**, 100101 (2008).
[25] Y.-H. Chu, M. P. Cruz, C.-H. Yang, L. W. Martin, P.-L. Yang, J.-X. Zhang, K. Lee, P. Yu, L.-Q. Chen, and R. Ramesh, Adv. Mater. **19**, 2662 (2007).
[26] X. Ke, P. P. Zhang, S. H. Baek, J. Zarestky, W. Tian, and C. B. Eom, Phys. Rev. B: Condens. Matter Mater. Phys. **82**, 134448 (2010).
[27] S. H. Baek, H. W. Jang, C. M. Folkman, Y. L. Li, B. Winchester, J. X. Zhang, Q. He, Y. H. Chu, C. T. Nelson, M. S. Rzchowski, X. Q. Pan, R. Ramesh, L. Q. Chen, and C. B. Eom, Nat. Mater. **9**, 309 (2010).
[28] W. C. Chen, R. Erwin, J. W. McIver III, S. Watson, C. B. Fu, T. R. Gentile, J. A. Borchers, J. W. Lynn, and G. L. Jones, Phys. B: Condens. Matter **404**, 2663 (2009).
[29] E. Lelièvre-Berna, E. Bourgeat-Lami, P. Fouilloux, B. Geffray, Y. Gibert, K. Kakurai, N. Kernavanois, B. Longuet, F. Mantegezza, M. Nakamura, S. Pujol, L.-P. Regnault, F. Tasset, M. Takeda, M. Thomas, and X. Tonon, Phys. B: Condens. Matter **356**, 131 (2005).
[30] M. Janoschek, S. Klimko, R. Gähler, B. Roessli, and P. Böni, Phys. B: Condens. Matter **397**, 125 (2007).
[31] See supplementary material at http://dx.doi.org/10.1063/1.4901294 for unpolarized neutron RSM.
[32] T. Chatterji, *Neutron Scattering from Magnetic Materials* (Elsevier Science, 2006).
[33] A. Poole and B. Roessli, J. Phys.: Conf. Ser. **340**, 012017 (2012).
[34] D. Sando, A. Agbelele, D. Rahmedov, J. Liu, P. Rovillain, C. Toulouse, I. C. Infante, A. P. Pyatakov, S. Fusil, E. Jacquet, C. Carrétéro, C. Deranlot, S. Lisenkov, D. Wang, J.-M. Le Breton, M. Cazayous, A. Sacuto, J. Juraszek, A. K. Zvezdin, L. Bellaiche, B. Dkhil, A. Barthélémy, and M. Bibes, Nat. Mater. **12**, 641 (2013).
[35] D. Rahmedov, D. Wang, J. Íñiguez, and L. Bellaiche, Phys. Rev. Lett. **109**, 037207 (2012).
[36] C. Madhu, M. B. Bellakki, and V. Manivannan, Indian J. Eng. Mater. Sci. **17**, 131 (2010), available at http://nopr.niscair.res.in/handle/123456789/8621.